



PAPER • OPEN ACCESS

Inert structural transition in 4H and 6H SiC at high pressure and temperature: a Raman spectroscopy study

To cite this article: Shuhou Maitani et al 2024 J. Phys. Commun. 8 065001

View the article online for updates and enhancements.

You may also like

- A sensitivity analysis of millimeter wave characteristics of SiC IMPATT diodes S K Swain, J Pradhan, G N Dash et al.
- Effect of hexagonality on the pressuredependent lattice dynamics of 4H-SiC Junran Zhang, Tao Liang, Yunhao Lu et al
- <u>Structure</u>, energetics, and electronic states of III–V compound polytypes Friedhelm Bechstedt and Abderrezak Belabbes

Journal of Physics Communications



OPEN ACCESS

RECEIVED

12 January 2024

REVISED

20 May 2024

ACCEPTED FOR PUBLICATION

4 June 2024

PUBLISHED

13 June 2024

Original content from this work may be used under the terms of the Creative Commons Attribution 4.0 licence

Any further distribution of this work must maintain attribution to the author(s) and the title of the work, journal citation



PAPER

Inert structural transition in 4H and 6H SiC at high pressure and temperature: a Raman spectroscopy study

Shuhou Maitani¹, Ryosuke Sinmyo¹, Takayuki Ishii² and Kenji Yoza³

- Department of Physics, School of Science and Technology, Meiji University, 1-1-1 Higashi Mita, Tama-ku, Kawasaki, Kanagawa, 214-8571, Japan
- Institute for Planetary Materials, Okayama University, 827 Yamada, Misasa, Tottori, 682-0193, Japan
- ³ Bruker Japan, K. K., Yokohama, Kanagawa, 221-0022, Japan

E-mail: smaitani@meiji.ac.jp

Keywords: SiC, Raman, phase transitions, high pressure, high temperature, diamond anvil cell, crystal structure

Supplementary material for this article is available online

Abstract

We conducted Raman spectroscopy measurements of 4H-SiC and 6H-SiC up to 69 GPa and 1023 K to assess the stability and bonding of SiC at high pressure and temperature. Both optic and acoustic modes were observed at wide pressure and temperature ranges. The temperature shifts of the Raman frequencies were fitted by the equation with the Bose–Einstein distribution function, and we found that the shifts were almost insensitive to the pressure. The mode Grüneisen coefficients weakly depend on the pressure and temperature, suggesting the sluggish transition of the crystal structure, unlike the previous experiments showing the transition or decomposition of SiC at high pressure and temperature conditions. Inert transitions are confirmed by Raman measurements and annealing experiments using multiple high-pressure apparatuses. The crystallinity may be a hidden critical parameter in the experiments to determine the stable polytypes of SiC under high pressure and temperature.

1. Introduction

Silicon carbides (SiC) draw great attraction to the industry as semiconductors for power electronics because of their wide band gaps and high blocking voltage [1]. Strong chemical bonding between silicon and carbon induces high hardness, thermal conductivity, and chemical inertness in the SiC [2]. The crystalline SiC is known to have many polytypes made by a combination of SiC_4 tetrahedra. They are usually described by using the Ramsdell notation [3]. SiC shows 3 C, 2H, 4H, 6H, 15 R, and so on at ambient pressure conditions. The polytypes of SiC consist of identical silicon (or carbon) layers but have different arrangements of these layers. The arrangements of the layers are formed by the twist of the SiC bonding, which rotates the SiC_4 tetrahedra. The crystal structures of 4H-SiC and 6H-SiC are illustrated in figure S1 using VESTA software[4]. The polytypes of SiC show a wide range of band gaps, from 2.39 eV of 3C-SiC to 3.33 eV of 2H-SiC [5]. The polytypism in SiC is thought to result from similar free energy among the crystal structures [6].

Nowadays, high-pressure treatment creates a new way to explore the novel crystal structure of the compounds [7]. One can expect that the underseen structure of SiC can be stable under high-pressure conditions. Therefore, the stability of the SiC polytypes has been studied at high-pressure conditions by means of *in situ* x-ray diffraction (XRD) measurements, Raman spectroscopy, and theoretical calculations (see [8] and references therein). Nevertheless, the phase diagram of SiC at high-pressure and -temperature conditions is not well constrained so far, likely because of the kinetics of the transition induced by strong covalent Si-C bonding [8]. Earlier XRD measurements showed that the 3C-SiC undergoes a phase transition to rocksalt type B1 structure (space group $Fm\bar{3}m$) at 100 GPa with a large decrease of the unit cell volume, in contrast to 6H being stable up to 95 GPa [9]. Later, the laser-heated diamond anvil cell experiments showed that the 3 C undergoes a phase transition to B1 structure at around 75 GPa and 2000 K by *in situ* XRD measurements [10]. On the

contrary, a similar experimental study showed that 3 C is decomposed into Si and C at around 60 GPa and higher temperature than 2000 K using high-pressure XRD measurements with laser-heated diamond anvil cells [11]. A previous study reported that the polytype of 6H-SiC partly keeps untransformed when a high-pressure polymorph of rocksalt-type structure appears during laser heating experiments above 2000 K [10]. The other previous study did not observe any phase transition in 3 C and 6H at 1–80 GPa and 1600–2200 K in the laser-heated diamond anvil cell experiments for a heating duration of ~14 min [12]. This discrepancy may be a result of the kinetics of the transition and/or unexpected chemical segregation caused by a large temperature gradient in the laser-heated diamond anvil cell [13]. Dynamic compression studies have been conducted to determine the crystal structure of the SiC under ultra-high pressure [14–16]. Previous studies in the crystal structure of SiC at high pressure were summarized in table S1. Together with the phase relationships, the equations of states of SiC were also studied in 3 C, 6H, and 4H by high-pressure experiments and theoretical calculations [8–10, 12, 17, 18]. The structure of SiC is fundamentally important in understanding the nature of the VI group semiconductors, which have broad applications [19].

Raman spectroscopy is an effective method for understanding solids' crystal structure and vibration modes of solids. Thus, the pressure and temperature evolution of the Raman frequency helps to understand the stability of the SiC polytypes. However, it has never been reported at high-pressure and -temperature conditions in the SiC. Previous studies reported the Raman frequencies of 3C-SiC [18], 4H-SiC [17], and 6H-SiC [20] at ambient temperatures up to 80, 55, and 95 GPa, respectively. A previous study suggested that Si-C bonding increases the ionicity with increasing pressure up to around 40 GPa, and then the bonding changes from ionic to covalent again at higher pressure based on the Raman spectroscopy measurements [20]. The study further predicted that 6H is unstable above around 100 GPa based on the decrease of mode Grüneisen coefficient at high pressure [20].

Recently, SiC has also been interested in geophysics and astrophysics as constituent materials of the Earth and planets [21, 22]. Enigmatic SiC found in nature is suggested to be created by the hydrogen-rich fluid arising from the subducted materials in the Earth's deep interior [21]. Although the Earth's mantle is mainly composed of silicate and oxide, recent studies showed that some extrasolar planets might have a larger C/O ratio above 1 [22]. While such carbon-rich planets are expected to be rare, SiC may be the main constituent material of the carbon-rich planets. The structure and dynamics of such exotic carbon-rich planets have been largely controlled by the stability and the physical properties of the SiC at high pressure [12, 23, 24]. However, the stability and bonding character of the polytypes of SiC under high pressure and temperature corresponding to the planetary interior are poorly understood.

Here, we have measured vibrational spectra of 4H-SiC and 6H-SiC at high pressure and temperature conditions by combining externally heated diamond anvil cells and laser Raman spectroscopy. Both optic and acoustic modes were observed at wide pressure and temperature ranges. Our new comprehensive Raman frequency data can help further analysis of the SiC sample in nature and in the laboratory as a reference. We did not observe any transition in the crystal structure within the experimental conditions. The Raman data and the annealing experiments showed the inertness of the transition between polytypes at high pressure and temperature, regardless of the heating methods. We conclude that the crystallinity may be a hidden critical parameter in the experiments to determine the stable polytypes of SiC.

2. Experimental procedures

We conducted high-pressure and high-temperature experiments using two types of high-pressure apparatus: a diamond anvil cell and a multi-anvil apparatus.

2.1. Diamond anvil cell experiments

We measured Raman spectra of SiC at high pressure and temperature conditions using a newly designed externally heated diamond anvil cell. Synthetic 4H-SiC and 6H-SiC were used as starting materials. 4H-SiC was a semi-insulating type single crystal grown on-axis (0001) with no dopant (electrical resistivity >0.1 $\mathrm{M}\Omega^*\mathrm{cm}$) and micro-pipe density of < 15 cm². 6H-SiC was a single crystal grown on-axis (0001) with a dopant of nitrogen (\sim 5*10¹⁸ cm³) and a micro-pipe density of < 30 cm². The samples were loaded into a diamond anvil cell for high-pressure experiments. The culets of the diamond anvils were 300 $\mu\mathrm{m}$ in diameter. The samples were put into the hole made in the rhenium gasket without a pressure medium to maximize the Raman signal at high temperature and high pressure (figure S2). The thickness of the gasket was initially \sim 50 $\mu\mathrm{m}$. After compression to the desired pressure, the samples were heated by an externally heated diamond anvil cell using a cylindrical graphite heater. The high-temperature field is stable and homogeneous by using a newly designed cylindrical heater. The diamond anvil cell was placed in the water-cooling vacuum chamber with optic glass suitable for the spectroscopic measurements to avoid the reaction of the heater with air. The water-cooling system minimized the pressure drift during heating, as shown in the previous study [25]. A stable DC power source (ZX-S-400LA,

Takasago) was used for heating with a ramp rate of about $10 \,\mathrm{K \, min}^{-1}$. It is known that the pressure possibly decreases or increases with increasing temperature in the externally heated diamond anvil cell experiments, likely because of the deformation of the gasket. In order to avoid the undesired change in the pressure, the cell was heated to 500 K and kept for several ten minutes before each experimental run. After repeating the procedure, the cell kept initial pressure after pre-heating experiments, suggesting the heating was an isochoric process. Once we confirmed that the pressure keeps the initial pressure, we conducted high-temperature experiments with Raman measurements. We held each high-temperature condition for 5 min during Raman measurements. Input power was 50 W at maximum for generating high temperatures up to 1023 K. We have subtracted the baseline in the Raman spectra using Spectra Manager software (JASCO Corporation). The temperatures were measured by a thermocouple attached to the surface of the diamond anvil. Type-K and W3% Re-W25%Re thermocouples were used for the experiments in 6H and 4H, respectively. The pressure was determined by using Raman spectra of the diamond anvil at 300 K [26]. To release the stress of the sample chamber, we conducted a pre-heating procedure <473 K before experiments. Once the pre-heating procedure was done, the sample pressure was the same before and after the heating experiments. The SiC samples were heated by an externally heated diamond anvil cell using a cylindrical graphite heater up to 1023 K at high pressure. Any damage in the heater and thermocouple was observed after heating experiments. Thermal pressure was estimated based on the methods proposed by the previous study based on an assumption of the isochoric [27]. We used thermoelastic parameters of SiC to be K = 243 GPa, K' = 2.79, dK/dT = -0.005 GPa K^{-1} , and $\alpha = 10^{-5}$ K $^{-1}$ for the estimation of the thermal pressure [12]. Raman spectroscopy measurements were conducted by confocal laser Raman spectrometer system (NRS-4500, JASCO) composed of a red enhanced CCD detector (DR324B, Andor) and Czerny–Turner type spectrometer (f = 200 mm) with 1800 G/mm grating. High spatial resolution along the laser axis was achieved (\sim 1.5 μ m) by the confocal microscope system used in NRS-4500. This is important for eliminating thermal emissions from the background. The laser was a TEM_{00} single mode 532 nm laser with an output of 50 mW. The exposure time was 30–180 s. The laser spot was focused on the sample surface to about 1 μ m in diameter. The Si standard was used for the calibration before and after experiments. After the heating experiments, we increased the pressure and then repeated the heating experiments. We conducted heating experiments at 15, 30, 45, and 60 GPa in 4H and at 25 and 67 GPa in 6H (table S2). We have conducted two separate runs, including six times of heating for the externally heated diamond anvil cell experiments in total.

The annealing experiment was conducted by a laser-heated diamond anvil cell. The single crystal 6H-SiC was put into the hole made in the rhenium gasket with NaCl as a pressure medium. The culets of the diamond anvils were 300 μ m in diameter. After compression, the sample was heated from a single side using a CW Fiber laser (TruFiber 200 P Compact, Trumpf). The flash heating experiment was conducted by the laser with a diameter > 100 μ m to cover the whole sample. We determined the temperature by a spectro-radiometric method using an EMCCD camera (ProEM HS: 512BX3, Princeton Instruments) attached to the spectrometer (IsoPlane-160, Princeton Instruments). The pressure was determined by using Raman spectra of the diamond anvil at 300 K [26]. The pressure was 16 GPa before and after the experiments. Raman spectroscopy measurements were conducted after annealing experiments. We conducted the single crystal XRD measurements in the recovered sample of ~100*60*10 μ m³. We used micro-focused x-ray diffractometers (D8 Venture, Bruker) with a target of Mo, set to 50 kV and 1.4 mA for single crystal XRD measurements. The software package APEX4 (Bruker) was used for data processing after the measurement, and SHELXL was used for crystal structure refinement [28]. During the analysis, the initial crystal structure, P63mc, for the refinement was set to the same one reported by the previous study in 6H-SiC [29].

2.2. Multi-anvil experiments

We used a reagent-grade SiC powder as a starting material for the multi-anvil experiments. The powder XRD measurements showed that the sample was mostly 6H-type SiC with a minor amount of 4H-type SiC (\sim 5%). One *in situ* high-pressure and high-temperature experiment at 10 GPa up to 2200 K was conducted using the 15-MN Kawai-type multi-anvil press with the Osugi guide block system [30], SPEED-Mk.II [31], at the BL04B1 beamline, in the synchrotron radiation facility, SPring-8, Japan. TF05 WC anvils with a truncation of 3.0 mm were used for the experiment in combination with an 8-mm Cr-doped MgO pressure medium. The cell assembly used in this study was designed with essentially the same concept as that reported by [32]. A LaCrO₃ cylindrical heater was set in a direction parallel to the incident x-rays. The starting sample was packed in a graphite cylindrical capsule with graphite lids at both ends. The cylindrical capsule was placed in the same direction as the cylindrical heater. A 25- μ m-thick Re cylindrical foil was placed out of the capsule. Electrical insulation between the heater and the Re foil was made by a MgO sleeve. A ZrO₂ thermal insulator was located outside the heater. Ta foils were electrically linked between both ends of the heater and second-stage anvil tops. MgO rods were placed at both ends of the sample capsule. Temperatures were monitored using a

 $W_{97}Re_3-W_{75}Re_{25}$ thermocouple at the surface of the Re foil, which was inserted into the heater normal to the x-ray incidence with an electrical insulator of alumina tubes. The temperature variation in the sample was estimated to be less than 5 K [33–35].

In situ energy-dispersive x-ray diffraction was performed using white x-rays, which were collimated to 50 μ m horizontally and 400 μ m vertically using two variable incident slits. Diffracted x-rays were collected at a 2 θ angle of ~6° for 150–300 s for a pressure marker of MgO outside the Re foil and the sample using a germanium solid-state detector (SSD) in an energy range of up to 130 keV. The channel-energy calibration of the SSD was made using the energies of the x-ray emission line (K α) of ⁵⁵Fe and the γ radiation from ⁵⁷Co and ¹³³Ba. The press was oscillated around the vertical axis between 0° and 6° during the x-ray diffraction measurements to suppress the heterogeneity of the intensities of the diffracted peaks [31]. Sample pressures were obtained from volumes of MgO using the MgO equation of state proposed by Tange et~al [36] based on the third-order Birch–Murnaghan equation of state.

The sample was first compressed to a press load of 2 MN (\sim 10 GPa) and heated to 2200 K at a rate of 100 K min⁻¹. During heating, we measured some x-ray diffraction patterns of MgO and the sample. At 1400 K, the sample pressure was decreased to \sim 9 GPa, and therefore we compressed it to 2.5 MN to keep the sample pressure of 10 GPa. At 2000 K, we kept the temperature for 30 min and took XRD patterns of the pressure marker and sample. We then further heated to 2200 K. After 1 min at 2200 K, the heater became electrically unstable and therefore we quenched the sample by switching off the applied electrical power. Then, the sample was decompressed to room pressure for 1 h.

3. Results

3.1. Raman measurements

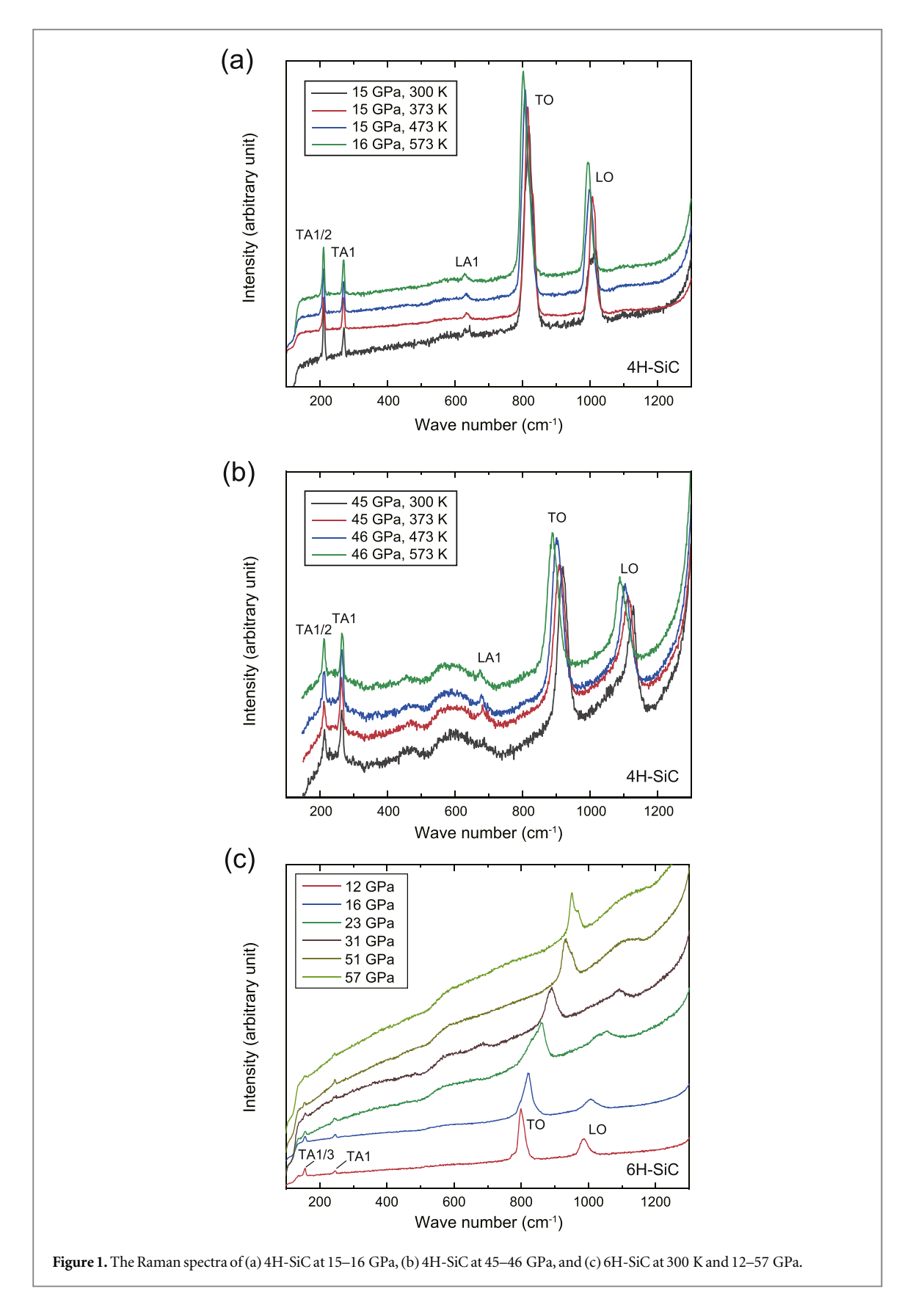
We have obtained the Raman spectra of 4H-SiC and 6H-SiC at high-pressure conditions up to 69 GPa (figure 1). Although we did not use a pressure medium in the externally heated diamond anvil cell, the full widths of the half maximum (FWHM) of the Raman peaks were relatively small at high pressure (figure 1). The observed Raman peaks were slightly asymmetric, possibly due to the Fano asymmetry [37, 38]. Although the asymmetry analysis will provide further information in the SiC, it will be beyond our current target. Figure 2 showed the Raman wavenumber against pressure at ambient temperature. The frequency of transverse optic (TO), longitudinal optic (LO), transverse acoustic (TA), and longitudinal acoustic (LA) modes are well consistent with the previous studies at ambient temperature [17, 20, 39]. The Raman spectra of the SiC polytypes are understood by large zones that extend in the axial direction to $N\pi/c$, where N is the number of layers in the polytype stacking sequence and c is the axial dimension of the unit cell. N are 6 and 4 in the 6H and 4H polytypes, respectively. Since $2\pi/c$ is a reciprocal lattice vector, the pseudo-momentum vectors $\mathbf{x} = \mathbf{q}/\mathbf{q}_{\text{max}} = 1/3, 2/3, 1$ for 6H and x = 1/2, 1 for 4H are equivalent to the Brillouin zone. Thus, accessible Raman scattering measurements are x = 1/2 and 1 for 4H, and x = 1/3, 2/3, and 1 for 6H [40, 41]. We have observed several acoustic modes in addition to TO and LO (figure 1). Observed acoustic modes were TA (x = 1/3 and 1) in the 6H and TA (x = 1/2 and 1) and LA (x = 1) in the 4H. The irreducible representation for the phonon modes were A_1 for LO, E₁ and E₂ for TO, A₁ for LA, E₁ for TA1, and E₂ for TA1/2 and TA1/3 [42, 43]. We have fitted the wavenumbers at high pressure and room temperature by the polynomial equations below

$$\omega_{i,P,300} = \omega_{i,0,300} + A^*P + B^*P^2 \tag{1}$$

where the ω_i is the wavenumber for i=TO, LO, TA, and LA modes, A and B are fitting parameters, and P is pressure in GPa. Fitting parameters are shown in table 1. TO, LO, and LA modes increase with increasing pressure, in contrast to TA modes. The pressure dependence of the frequencies is consistent with the previous studies [17, 20], while TA and LA modes were determined at high-pressure conditions for the first time in this study. In particular, very small or negative pressure dependence of TA modes have been noticed in 6H-SiC and 3C-SiC [42, 44]. Since the pressure dependences of the wavenumber are almost linear, we additionally fitted the data by a linear function. We fitted all data, low-pressure data, and high-pressure data, separately (Table S3 and figure S3).

During the experiments at high temperatures, the frequencies of the optic Raman modes were observed to decrease with increasing temperature (figure 3). The signal-to-noise ratios are sufficiently high for the determination of the effect of temperature in the vibrational frequency at high pressure (figure 1). Figure 4 shows the difference of high-temperature wavenumbers with respect to $\omega_{LO,P,300}$. It is clearly shown that the temperature dependence of the wavenumbers is almost the same at any pressure conditions (figure 4). The temperature shifts of the wavenumbers (ΔT) are fitted into the equations with the Bose–Einstein distribution function $n(T, \omega)$ as shown below [43, 45]

$$\Delta T = C[1 + 2n(T, \omega_{i,0,0}/2)] + D[1 + 3n(T, \omega_{i,0,0}/3) + 3n^2(T, \omega_{i,0,0}/3)]$$
(2)



$$n(T, \omega) = 1/[\exp(h\omega/k_BT) - 1]$$

where the $\omega_{i,0,0}$ is wavenumber at 1 atm and 0 K, T is the temperature in K, h is the Plank constant, and k_B is the Boltzmann constant. The obtained results at high pressure are generally in good agreement with the previous study at 1 atm [43]. Our new high-pressure data showed that the temperature parameters C and D were insensitive to the pressure (figure 4). The values of C, D, and $\omega_{i,0,0}$ of 4H were -0.34, -7.7, and 974.8 cm⁻¹

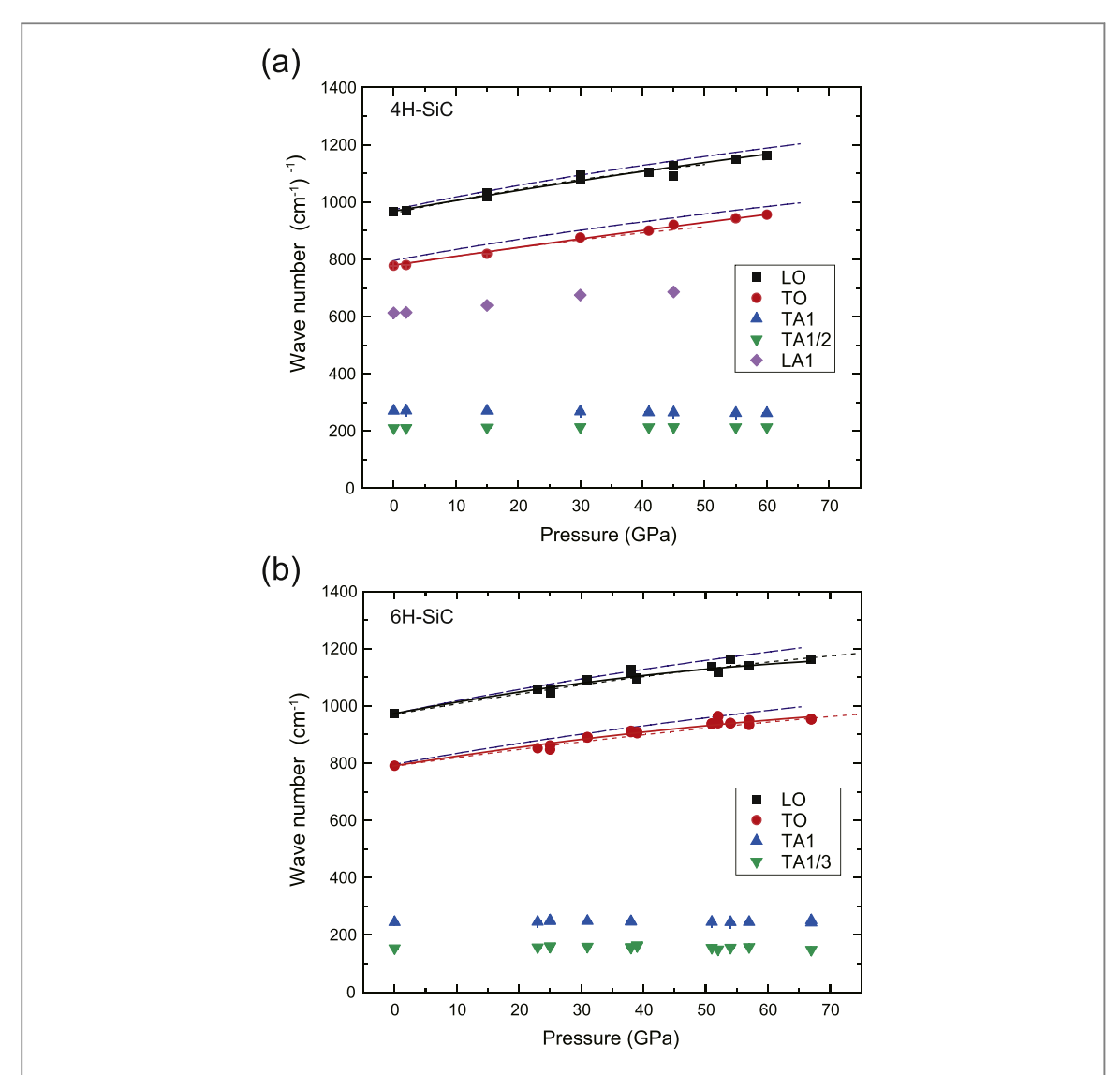


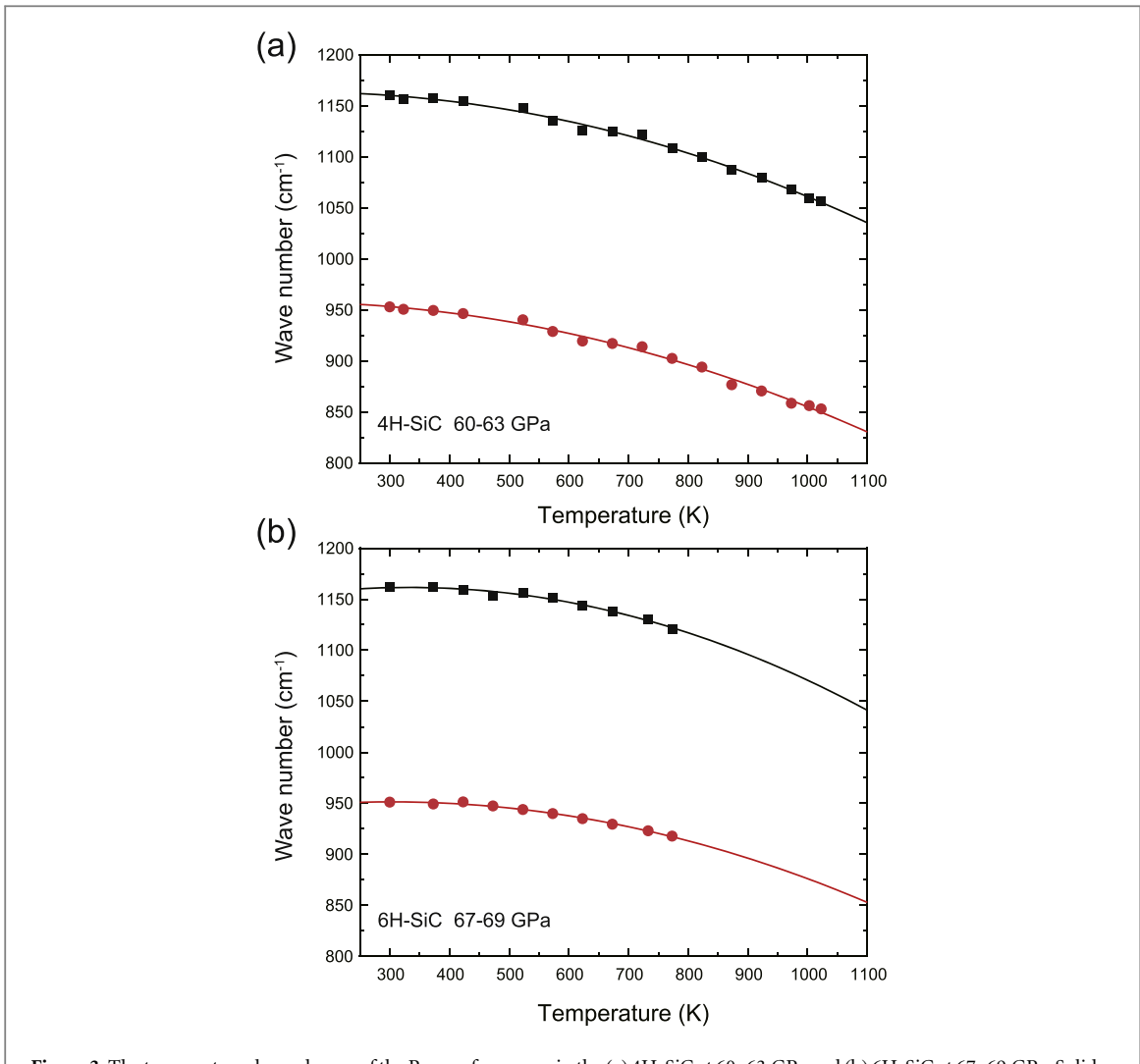
Figure 2. The relationships between pressure and the Raman frequency at 300 K in the (a) 4H-SiC and (b) 6H-SiC. All symbols are results obtained by this study. Black and red solid lines = fitted curves (this study); black and red dotted lines = previous studies in 4H-SiC [17] and 6H-SiC [20]. Blue broken lines are 3C-SiC for comparison [18]. The lines are drawn within the experimental conditions.

Table 1. Pressure dependencies on the Raman wavenumber of SiC.

		$A (cm^{-1}*GPa^{-1})$	$B(\mathrm{cm}^{-1*}\mathrm{GPa}^{-2})$
4H-SiC	LO	3.8(2)	$-8.0(40)^*10^{-3}$
	TO	3.2(2)	$-4.1(40)^*10^{-3}$
	LA1	1.7(1)	_
	TA1	$-1.3(1)^*10^{-1}$	_
	TA1/2	$-6.7(7)^*10^{-2}$	_
6H-SiC	LO	4.2(4)	$-2.2(7)^*10^{-2}$
	TO	3.5(3)	$-1.4(7)^*10^{-2}$
	TA1	$6.1(16)^*10^{-2}$	_
	TA1/3	$9.3(32)^*10^{-2}$	_

 $(R^2=0.98)$ for LO, and 4.7, -5.5, and 779.9 cm $^{-1}$ ($R^2=0.99$) for TO. The values of 6H were 52, -13, and 937.0 cm $^{-1}$ ($R^2=0.95$) for LO and 29, -7.0, and 770.8 cm $^{-1}$ ($R^2=0.98$) for TO. A recent study has shown that the FWHM of Raman peaks contains information on the temperature [38]. Since it can be a good measure of the temperature using Raman spectroscopy, asymmetry analysis should be done in future studies.

During heating at a higher pressure than \sim 30 GPa, broad Raman peaks were observed at around 600 cm⁻¹ in addition to the initially observed peaks (figure 1). This may be second-order LA peaks around 500–700 cm⁻¹ in 3 C [46], 4H [47], or 6H [42]. Since the wavenumbers of LO and TO are clearly different from the values of 3 C



 $\textbf{Figure 3.} \ \ \text{The temperature dependences of the Raman frequency in the (a) 4H-SiC at 60-63 \ \ GPa \ \ and (b) 6H-SiC at 67-69 \ \ GPa. \ \ Solid curves are fitted results by the equations with the Bose-Einstein distribution function (see text). }$

[18], the 6H and 4H polytypes persist in their original crystal structure up to high temperatures of 773 K and 1023 K.

3.2. Annealing experiments

The results of multi-anvil experiments showed that the 6H polytype mostly keeps the original structure, up to 2000 K at 10 GPa for 30 min (figure S4). Any additional phases, such as silicon and diamond, are not observed during heating. Obtained unit cell parameters of 6H-SiC were a = b = 3.065(1) Å, c = 15.00(3) Å, and V = 122.0(7) Å³ at 10 GPa and 2000 K. The flash annealing experiment by laser-heated diamond anvil cell also showed that the 6H polytype remains untransformed after heating at 16 GPa. The optical microscopic images of samples are shown in figure S5. The temperatures were 2400(300) K and 2200(100) K on the laser-irradiated side and the other side, respectively. The errors were the standard deviation of the temperature within the sample. The pressure was estimated to be 22 GPa at 2300 K after the thermal pressure correction [27]. The heating duration was ~150 milliseconds according to the continuous measurements of the spectra-radiometry. Raman measurements showed that no additional phases exist other than 6H-SiC after experiments. We conducted the single crystal XRD measurements in the starting material and recovered sample after laser-heated diamond anvil cell experiments (Tables S4 and S5). We obtained 829 reflections, including 139 independent reflections for the sample after heating. A reference structure of a = b = 3.0810(2) Å, c = 15.1248(10) Å, and $V = 124.338(14) \text{ Å}^3$ were taken from Capitani et al [28]. We obtained almost same crystal structures of the starting materials, $a = b = 3.08060(10) \text{ Å}, c = 15.1151(9) \text{ Å}, and <math>V = 124.226(11) \text{ Å}^3$ by a single crystal XRD measurement at ambient condition. The results of the refinement analysis showed unit cell parameters were a = b = 3.0782(11) \mathring{A} , c = 15.102(8) \mathring{A} , and V = 123.92(11) \mathring{A}^3 at ambient conditions with an R-value of 3.7%. The cell parameters and atomic positions were similar to the initial crystal structure, while the c-axis and volume of the unit cell were slightly lower than that of the initial value [29].

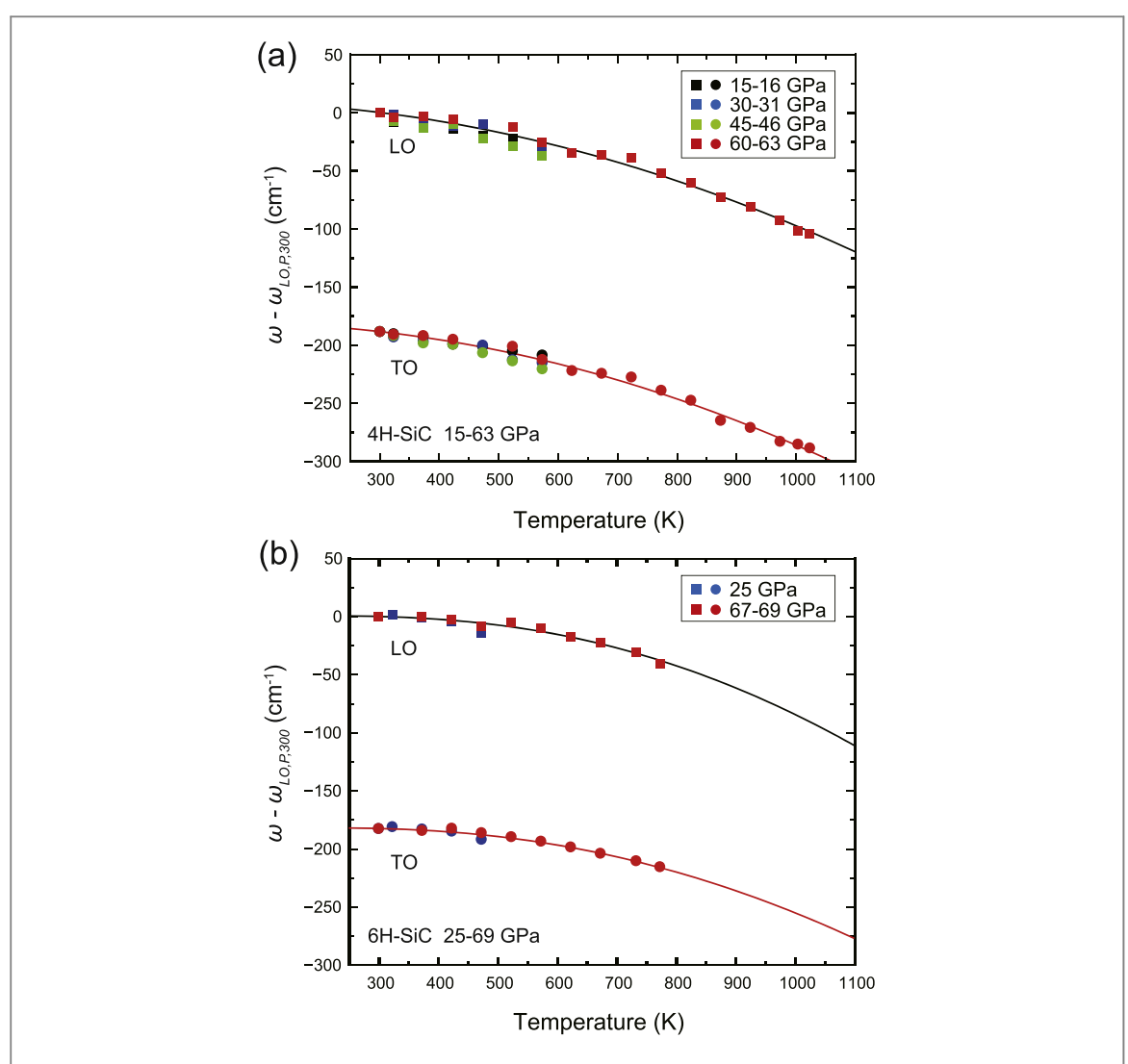


Figure 4. The effect of the temperature on the Raman frequency of (a) 4H-SiC at 15–63 GPa and (b) 6H-SiC at 25–69 GPa. The wavenumbers were normalized to the value of LO at 300 K at given pressures $\omega_{LO,P,300}$. The lines are fitted curves by the equations with the Bose–Einstein distribution function (solid).

4. Discussions

4.1. Pressure dependence of the Raman frequency

Pressure dependence of the Raman frequency provides insight into the bonding of the Si and C at high-pressure conditions. Moreover, it can be a pressure standard during high-pressure experiments. Peaks of optic modes (LO and TO) are much stronger than those of the acoustic modes and are sensitive to pressure (figures 1 and 2). TO is always the most intense and sensitive to pressure; thus, it is the most suitable mode as a pressure marker in the diamond anvil cell. The LO-TO peak splitting indicates the change in the covalent bonding in the SiC [20]. According to a previous study, the covalent character decreases with increasing pressure up to 70 GPa [20]. Current results showed a similar trend with previous studies in the 6H and 4H (figure 5) [17, 20]. Figure 5(a) summarizes the LO-TO splitting at high-pressure conditions and 300 K. 4H and 6H showed a similar trend in the LO-TO splitting against pressure (figure 5(a)). Our new high-temperature data showed that LO-TO splitting is less sensitive to temperature compared to the effect of pressure (figure 5(b)). The splitting keeps an almost constant value or weakly decreases with temperature. The scattered data in 6H-SiC may result from uncertainty in the pressure determination and undesired uniaxial stress [48], which are unfortunately not straightforward to investigate with the experimental setup in this study and previous study [20]. The transverse effective charge was calculated by following previous literature [17, 20, 39].

$$\omega_{LO}^2 - \omega_{TO}^2 = \frac{4\pi e_T^{*2}}{\varepsilon_\infty \mu V_a} \tag{3}$$

where e_T^* is transverse effective charge, ε_∞ is the dielectric constant at high frequency, μ is the reduced mass, and V_a is the volume per atom. $\varepsilon_\infty = 6.52$ was used for the value at ambient pressure, and their pressure

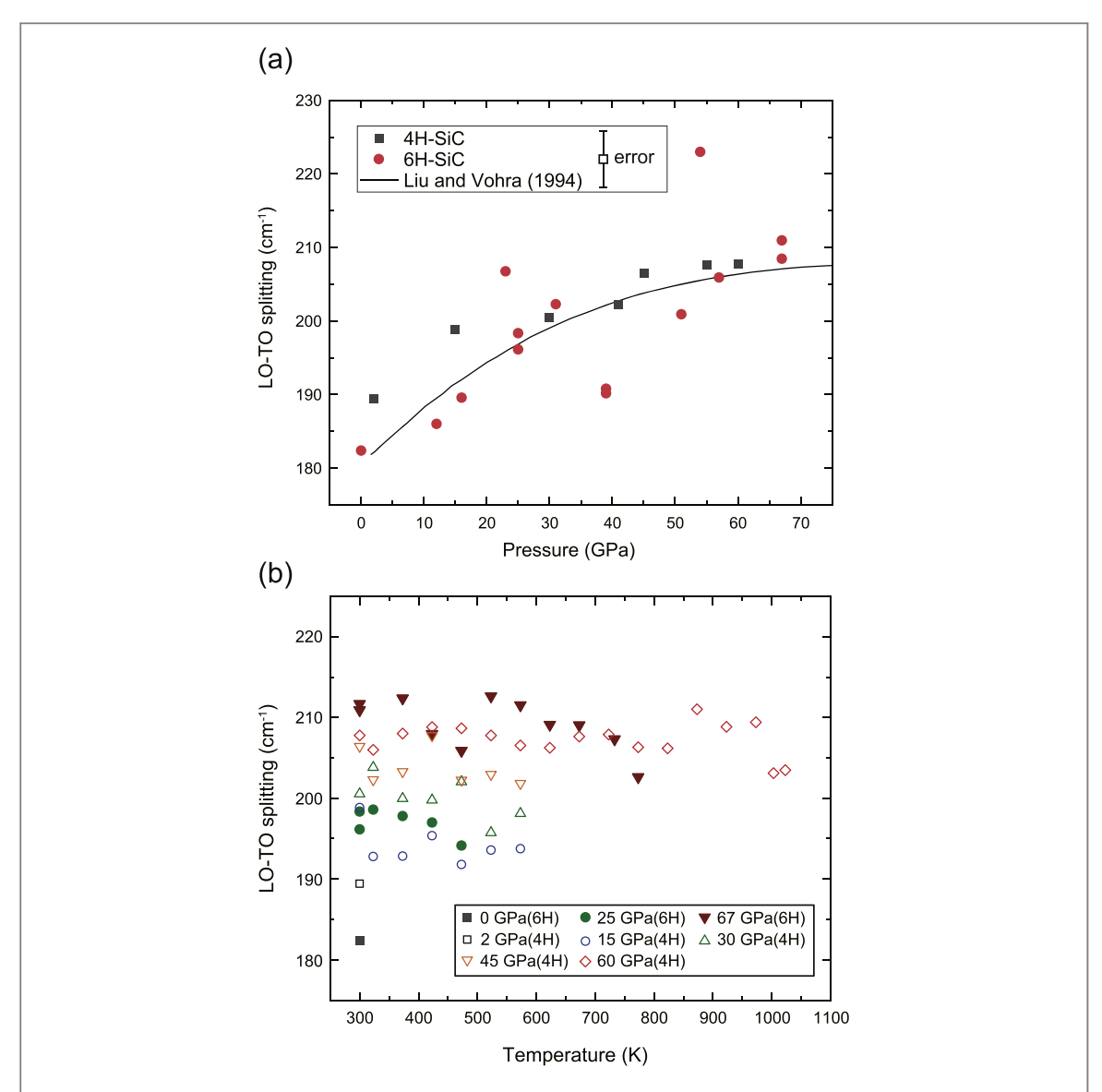


Figure 5. (a) The LO-TO splitting in 4H-SiC (black) and 6H-SiC (red) at high-pressure conditions and 300 K (this study). The solid line is taken from the previous study in 6H-SiC [20]. Typical error was estimated by the FWHM of the literature [20]. (b) The LO-TO splitting in 4H-SiC (open symbols) and 6H-SiC (filled symbols) at high pressure and temperature conditions.

dependences $r = d \ln \varepsilon_{\infty}/d \ln V_a$ were varied from 0, 0.3, 0.6, to 1 [17] (figure 6). The obtained results clearly showed that pressure plays an important role on the effective charge of SiC. However, it is also obvious that the dielectric constant should be determined at high pressure for a better understanding of the ionic/covalent future of the SiC. On the other hand, current results suggested that the covalency of the bonding is not altered at high temperatures, at least up to 1023 K, in contrast to the effect of pressure [20].

6H is predicted to be unstable above \sim 100 GPa based on the anomalous decrease of mode Grüneisen coefficient γ_i of the LO and TO phonons compared to the other tetrahedrally coordinated semiconductors, such as diamond and cBN [20]. The mode Grüneisen coefficient for the discussion above was defined as

$$\gamma_i = \frac{d \ln \omega_i}{d \ln V} \tag{4}$$

where V is volume [20]. We have used the equations of state of 6H [9] and 4H [17] to calculate γ_i . The obtained values are summarized in table 2. Obtained slopes of the γ_i value of 4H and 6H as a function of the density are much shallower than in the previous study (figure S6), suggesting that the LO and TO modes are harder than in the previous estimation under high pressure. Current results showed that the 4H and 6H are similar to the diamond and cBN, showing constant γ_i value at high-pressure conditions. The constant γ_i value suggests that the experimental pressure was not sufficiently high for the transition. This is supported by the experimental results showing no transition in the crystal structure at high pressure and temperature, as shown by this study and a previous study [12]. We should note here that the γ_i value may have large uncertainties because it is the second-order derivative of the experimental data, as already described in the previous study [17, 20].

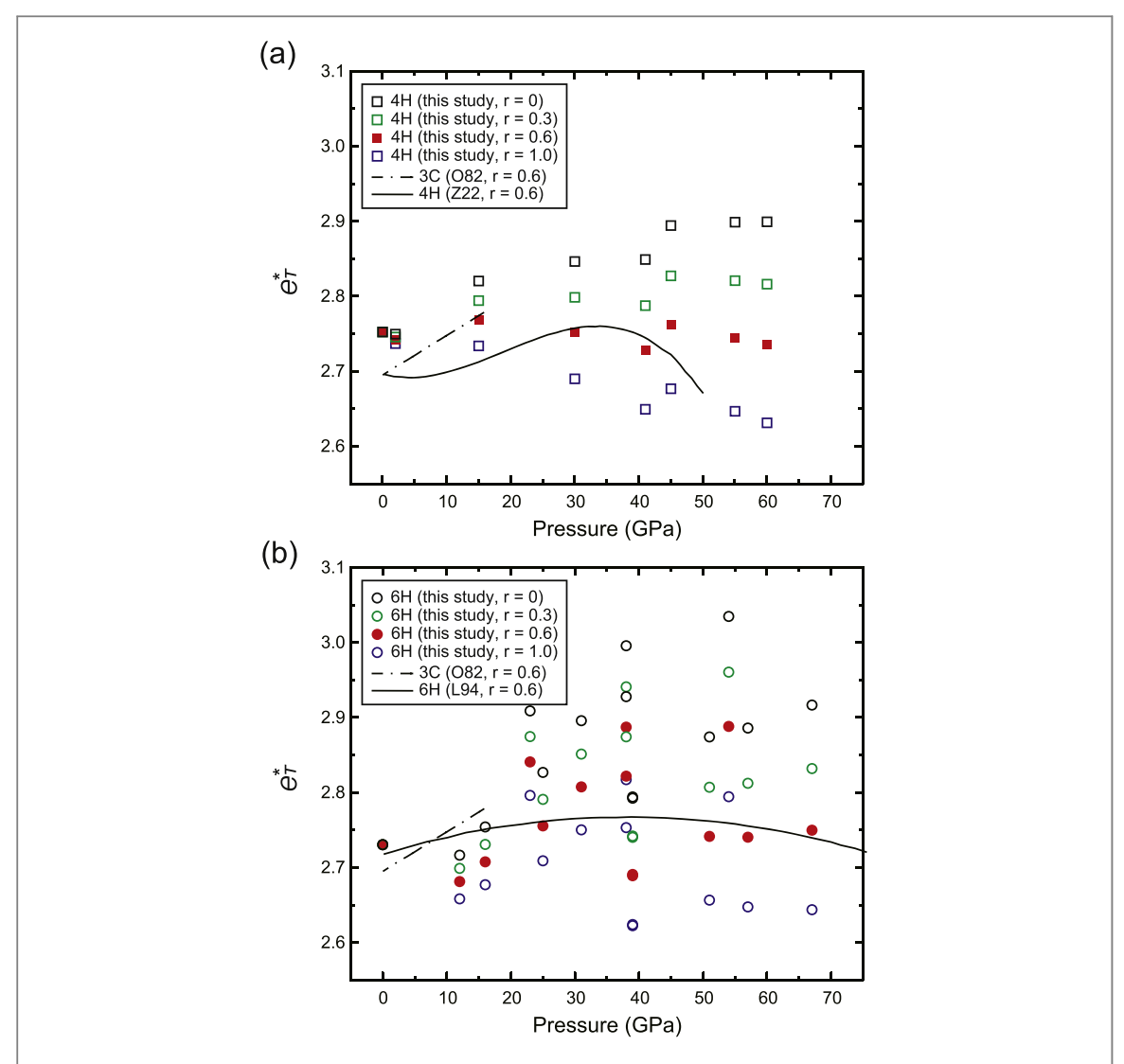


Figure 6. Transverse effective charge of (a) 4H-SiC and (b) 6H-SiC at high pressure and 300 K. Symbols are data obtained by this study, and lines are taken from the literature [17, 20, 39]. The data with r = 0.6 (see text) are highlighted for a comparison with previous data.

Table 2. Mode Grüneisen coefficients γ_i of SiC.

	4H-SiC	6H-SiC
LO	0.90(9)	0.97(20)
TO	0.96(11)	1.1(3)
LA1	0.53(7)	_
TA1	0.0054(27)	0.044(24)
TA1/3	_	0.081(57)
TA1/2	-0.010(3)	_

The obtained value of TA mode (x = 1) does not largely change at high pressure and high temperatures to 69 GPa and 773 K (table 2, figure 7 and S7). The small negative γ_i value of TA mode (x = 1) suggests that the transitions to other polytypes are sluggish because the TA mode (x = 1) corresponds to the intercell vibration of the atoms [42]. The insensitive γ_i value against pressure and temperature of TA is an explanation for the inert transition between polytypes in the high-pressure and -temperature experiments even above 2000 K [10, 12].

4.2. Temperature dependence of the Raman frequency

We have obtained the Raman spectra at high temperatures up to 1023 K at high pressure. As temperature increases, the wavenumber of LO and TO decreases, and the temperature shifts are almost the same at any

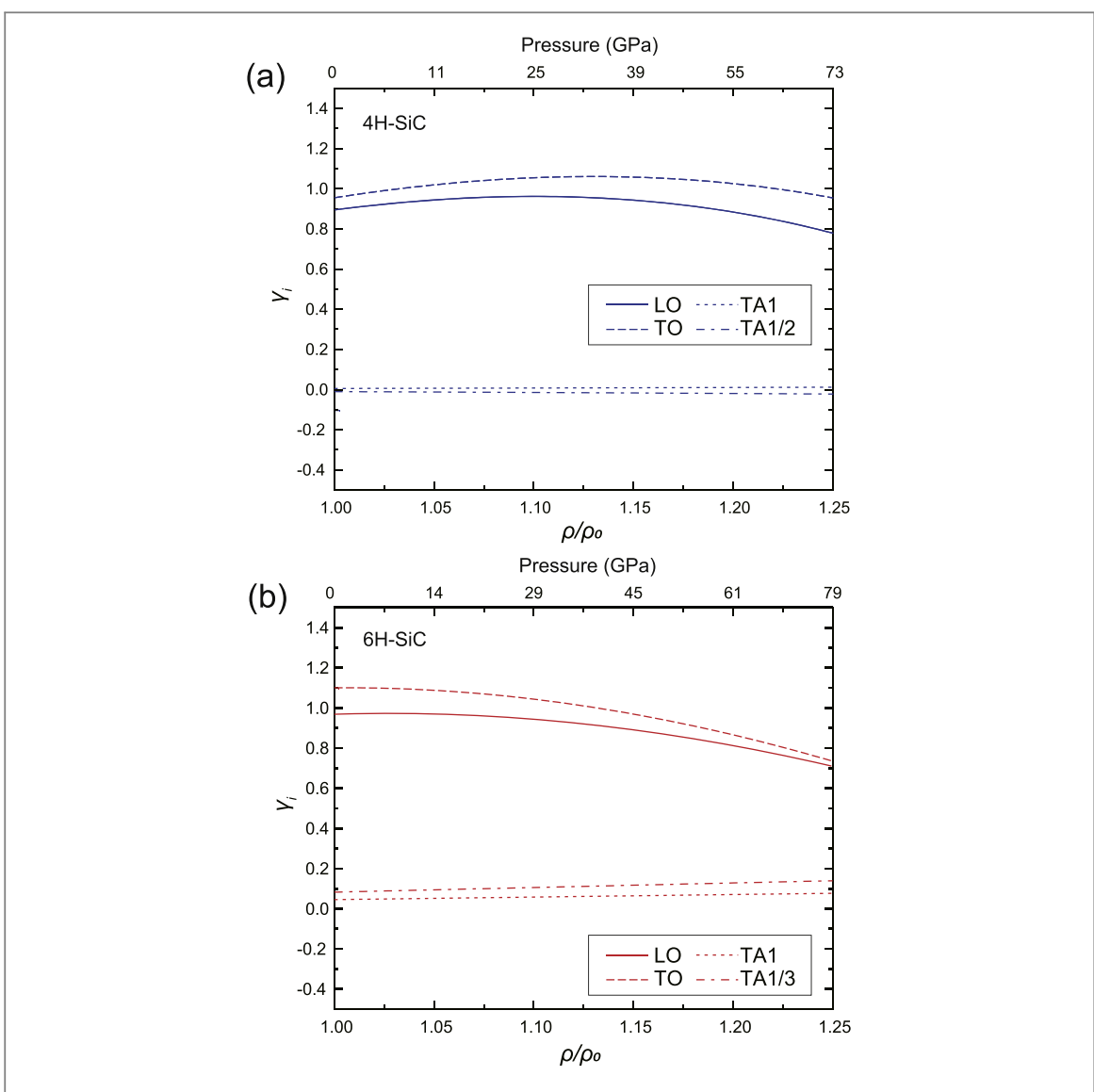


Figure 7. The mode Grüneisen coefficient γ_i of the LO (solid lines), TO (broken lines), and TA (dotted lines and dash-dot-dash lines) modes of (a) 4H-SiC and (b) 6H-SiC at high pressure and 300 K.

pressure conditions (figure 4). The peak shifts are more significant at higher temperatures in both 4H and 6H. The model with the Bose–Einstein distribution function well fits the temperature dependences of the frequencies in this study (figure 4). TO mode shows the peak shift of $\sim -10~\rm cm^{-1}$ per 100 K. This value is much higher than the zircon and quartz, which is widely used as a pressure and temperature marker in the diamond anvil cell experiments [49, 50]. Therefore, TO mode may be useful for a pressure and temperature marker in the diamond anvil cell at a higher pressure than several 10 GPa. Although the peak shift against the pressure is smaller than that of zircon and quartz [49, 50], SiC has a great advantage in the wide applicable pressure and temperature range. Moreover, the SiC may be stable under very reducing conditions compared to the oxides. The SiC may be a good pressure and temperature marker in the diamond anvil cell experiments in addition to the 13 C-enriched diamond and the cBN [51–53].

The anharmonic mode parameter a_i is used to estimate the anharmonicity of the modes [54, 55].

$$a_{i} = \alpha(\gamma_{iT} - \gamma_{iP})$$

$$\gamma_{iT} = \left(\frac{K_{T}}{\omega_{i0}}\right) \left(\frac{\partial \omega_{i}}{\partial P}\right)_{T}$$

$$\gamma_{iP} = -\left(\frac{1}{\alpha \omega_{i0}}\right) \left(\frac{\partial \omega_{i}}{\partial T}\right)_{P}$$

$$(5)$$

where α is the thermal expansion coefficient, and K_T is the bulk modulus. We have used a bulk modulus of 213.61 GPa for 4H [17] and 260 GPa for 6H [9]. This time, α is assumed to be 1*10⁻⁵ for both 4H and 6H. The a_i parameters are summarized in table 3. In the harmonic and quasi-harmonic approximation, $\gamma_{iT} = \gamma_{iP}$ and thus

Table 3. Mode Grüneisen coefficients (γ_{iT} and γ_{iP}) and anharmonic parameter of SiC.

		4H-SiC		6H-SiC		
	γ iT	γ iP	$a_i(10^{-5})$	γ iT	γ iP	$a_i(10^{-5})$
LO	0.76(34)	9.5(8)	-8.7(9)	0.84(25)	3.8(20)	-3.0(20)
TO	0.84(16)	10(1)	-9.5(6)	0.90(2)	3.4(26)	-2.5(25)
LA1	0.53(7)	8.0(6)	-7.5(7)	_		_
TA1	0.0050(30)	0.21(30)	-0.20(30)	0.044(20)	1.5(52)	-1.5(51)
TA1/3	_	_	_	0.081(52)	1.0(12)	-1.0(13)
TA1/2	-0.010(3)	1.8(4)	-1.8(4)	_	_	_

 $a_i = 0$ [54, 55]. Deviation of the a_i parameters from zero indicates that the quasi-harmonic approximation is inappropriate for the modes. Obtained a_i parameters of SiC are comparable with the silicates, such as α -quartz and coesite, reported previously [55]. The current results showed an apparent deviation of the parameters from zero in the LO, TO, and LA modes compared to the TA, suggesting that the anharmonic behavior is stronger in the LO, TO, and LA. The harmonic and quasi-harmonic approximation may not correctly predict the thermoelastic parameters of the SiC under planetary interior conditions. The modification of mode in SiC may help understand the nature of the VI group semiconductors [19, 56].

4.3. Stability of the SiC polytypes under high pressure and temperature

Obtained TA (x = 1) mode, corresponding to the intercell vibration, was insensitive to the pressure and temperature in both 4H and 6H (figure 7 and S7). This suggests that the transition of the crystal structure of SiC may require higher pressure and temperature than the experimental conditions [42]. The obtained γ_i value also indicates the strong kinetic barrier hindering the phase transition in the crystal structure of SiC polytypes. We conducted annealing experiments using the multi-anvil and laser-heated diamond anvil cell to test the inertness of the transition further. It is known that the multi-anvil can generate a stable and homogeneous temperature field compared to the laser-heated diamond anvil cell experiments. The multi-anvil press experiment showed that 6H-SiC mostly remains the crystal structure at 10 GPa and 2000 K for 30 min. The result is consistent with the earlier quench experiments by large-volume press (Whitney *et al* 1969). The laser-heated diamond anvil cell experiments showed that the crystal structure of the 6H-SiC was very similar to the original structure even after being annealed under a relatively large temperature gradient (Table S4 and S5). Our results are consistent with a previous study using laser-heated diamond anvil cells [12], while they contradict the other studies [10, 11]. The discrepancy among the diamond anvil cell studies may be due to chemical heterogeneity caused by the laser heating method [13], in addition to the kinetics of the transition between the polytypes having similar free energy [57].

The sluggish phase transition is commonly observed in highly covalent materials, such as diamond and related phases [58]. By analogy with the diamond, the transition of SiC is controlled by various experimental conditions, such as heating duration, heterogeneity in the temperature, stress, and the crystallinity of the starting materials. Although we have conducted single-sided laser heating experiments to enhance the effect of the heterogeneity in the temperature, we did not observe the transition. This result indicates that the temperature gradient may not be a dominant factor, at least to the degree of several hundred K per 10 micrometers. In addition to the temperature heterogeneity, the crystal disorder, such as dislocation and stacking fault, can also be an important factor in the transition, although previous studies did not pay much attention to the crystallinity of the starting materials. We used a single crystal with very low dislocation density (micro-pipe density of <15 cm²) as a starting material this time. The density of dislocation or stacking faults may increase due to the deformation under uniaxial compression in the diamond anvil cell, in contrast to the multi-axial compression in the multi-anvil press. Accordingly, the crystal disorder may be the dominant factor in the transition of the SiC in the high-pressure experiments.

5. Conclusions

We conducted Raman spectroscopy measurements in 4H-SiC and 6H-SiC up to 69 GPa and 1023 K. Both optic and acoustic modes were observed at wide pressure and temperature ranges. The pressure and temperature shifts of the Raman frequencies were fitted using the polynomial and the Bose–Einstein distribution functions, respectively. SiC may be a good pressure and temperature marker in the diamond anvil cell experiments. The mode Grüneisen coefficients were insensitive to the pressure and temperature, suggesting the inert structural

transition in 4H-SiC and 6H-SiC at high pressure and temperature. The results of annealing experiments also supported inert transitions.

Acknowledgments

We appreciate two anonymous reviewers for their fruitful comments. S M was supported by the Sasakawa Scientific Research Grant from The Japan Science Society. R S was supported by the KAKENHI Grant Numbers 19H01989 and 23H01277. T I was supported by the KAKENHI Grant Numbers 23K19067 and 24K00735. The synchrotron x-ray diffraction experiment was performed at the BL04B1 beamline at SPring-8 with the approval of the Japan Synchrotron Radiation Research Institute (Proposal No. 2023A1210). This paper presents results of a joint research program carried out at the Institute for Planetary Materials, Okayama University, supported by 'Joint Usage/Research Center' program by MEXT, Japan (No. G23–008).

Data availability statement

All data that support the findings of this study are included within the article (and any supplementary files).

ORCID iDs

Shuhou Maitani https://orcid.org/0009-0009-5220-5626

References

- [1] Cooper J A and Agarwal A 2002 SiC power-switching devices-the second electronics revolution? Proc. IEEE 90 956-68
- [2] Kimoto T 2015 Material science and device physics in SiC technology for high-voltage power devices Jpn. J. Appl. Phys. 54 040103
- [3] Ramsdell L S 1947 Studies on silicon carbide Am. Mineral. 32 64-82
- [4] Momma K and Izumi F 2011 VESTA 3 for three-dimensional visualization of crystal, volumetric and morphology data J. Appl. Crystallogr. 44 1272–6
- [5] Ivanov P and Chelnokov V 1992 Recent developments in SiC single-crystal electronics Semicond. Sci. Technol. 7 863
- [6] Park C, Cheong B-H, Lee K-H and Chang K-J 1994 Structural and electronic properties of cubic, 2H, 4H, and 6H SiC *Phys. Rev.* B 49 4485
- [7] Dubrovinsky L et al 2022 Materials synthesis at terapascal static pressures Nature $605\,274-8$
- [8] Daviau K and Lee K K M 2018 High-pressure, high-temperature behavior of silicon carbide: a review Crystals 8 217
- [9] Yoshida M, Onodera A, Ueno M, Takemura K and Shimomura O 1993 Pressure-induced phase transition in SiC Phys. Rev. B: Condens. Matter 48 10587-90
- [10] Kidokoro Y, Umemoto K, Hirose K and Ohishi Y 2017 Phase transition in SiC from zinc-blende to rock-salt structure and implications for carbon-rich extrasolar planets *Am. Mineral.* **102** 2230–4
- [11] Daviau K and Lee K K M 2017 Decomposition of silicon carbide at high pressures and temperatures Phys. Rev. B 96 174102
- [12] Nisr C, Meng Y, MacDowell A A, Yan J, Prakapenka V and Shim S H 2017 Thermal expansion of SiC at high pressure-temperature and implications for thermal convection in the deep interiors of carbide exoplanets *Journal of Geophysical Research: Planets* 122 124–33
- [13] Sinmyo R and Hirose K 2010 The Soret diffusion in laser-heated diamond-anvil cell Phys. Earth Planet. Inter. 180 172-8
- [14] Sekine T and Kobayashi T 1997 Shock compression of 6H polytype SiC to 160 GPa Phys. Rev. B 55 8034
- [15] Tracy S J et al 2019 In situ observation of a phase transition in silicon carbide under shock compression using pulsed x-ray diffraction Phys. Rev. B 99 214106
- [16] Kim D et al 2022 Structure and density of silicon carbide to 1.5 TPa and implications for extrasolar planets Nat. Commun. 13 2260
- [17] Zhang J et al 2022 Effect of hexagonality on the pressure-dependent lattice dynamics of 4H-SiC New J. Phys. 24 113015
- [18] Zhuravlev K K, Goncharov A F, Tkachev S N, Dera P and Prakapenka V B 2013 Vibrational, elastic, and structural properties of cubic silicon carbide under pressure up to 75 GPa: implication for a primary pressure scale *J. Appl. Phys.* 113 113503
- $[19] \ \ Xu\ K\ 2016\ Integrated\ silicon\ directly\ modulated\ light\ source\ using\ p-well\ in\ standard\ CMOS\ technology\ \emph{IEEE Sens. J.}\ 16\ 6184-91$
- [20] Liu J and Vohra Y K 1994 Raman modes of 6 h polytype of silicon carbide to ultrahigh pressures: a comparison with silicon and diamond *Phys. Rev. Lett.* **72** 4105
- [21] Bali E, Audetat A and Keppler H 2013 Water and hydrogen are immiscible in Earth's mantle Nature 495 220-2
- [22] Madhusudhan N, Lee K K M and Mousis O 2012 A possible carbon-rich interior in super-earth 55 cancri e Astrophys. J. Lett. 759 L40
- [23] Daviau K and Lee K K M 2017 Zinc-blende to rocksalt transition in SiC in a laser-heated diamond-anvil cell Phys. Rev. B 95 134108
- [24] Daviau K, Meng Y and Lee K K M 2019 SiO2-SiC Mixtures at High Pressures and Temperatures: implications for Planetary Bodies Containing SiC Journal of Geophysical Research-Planets 124 2294–305
- [25] Zhang Y, Wu Y, Han Y and Gao Y 2022 Water-cooling diamond anvil cells: an approach to temperature-pressure relation in heated experiments Rev. Sci. Instrum. 93 103904
- $[26]\ Akahama\ Y\ and\ Kawamura\ H\ 2006\ Pressure\ calibration\ of\ diamond\ anvil\ Raman\ gauge\ to\ 310\ GPa\ \emph{J.\ Appl.\ Phys.}\ 100\ 043516$
- [27] Andrault D et al 1998 Thermal pressure in the laser-heated diamond-anvil cell: an x-ray diffraction study Eur. J. Mineral. 10 931–40
- [28] Sheldrick G M 2008 A short history of SHELX Acta Crystallogr., Sect. A 64 112–22
- [29] Capitani G C, Di Pierro S and Tempesta G 2007 The 6H-SiC structure model: further refinement from SCXRD data from a terrestrial moissanite Am. Mineral. 92 403–7
- [30] Ishii T, Liu Z and Katsura T 2019 A breakthrough in pressure generation by a Kawai-type multi-anvil apparatus with tungsten carbide anvils Engineering 5 434—40

- [31] Katsura T et al 2004 A large-volume high-pressure and high-temperature apparatus for in situ x-ray observation, 'SPEED-Mk.II' Phys. Earth Planet. Inter. 143 497–506
- [32] Chanyshev A et al 2022 Depressed 660-km discontinuity caused by akimotoite-bridgmanite transition Nature 601 69-73
- [33] Ishii T et al 2018 Complete agreement of the post-spinel transition with the 660-km seismic discontinuity Sci. Rep. 8 6358
- [34] Ishii T et al 2019 Sharp 660-km discontinuity controlled by extremely narrow binary post-spinel transition Nat. Geosci. 12 869-72
- [35] Katsura T et al 2003 Post-spinel transition in Mg2SiO4 determined by high P-T in situ x-ray diffractometry Phys. Earth Planet. Inter. 136 11–24
- [36] Tange Y, Nishihara Y and Tsuchiya T 2009 Unified analyses for P-V-T equation of state of MgO: a solution for pressure-scale problems in high P-T experiments *J. Geophys. Res.* 114 B03208
- [37] Bhattacharjee S and Chattopadhyay K K 2022 Laser-induced Fano asymmetry, electron–phonon coupling, and phase transition in lanthanide sesquioxide (Ln2O3; Ln = Eu, Gd, Dy) nanoparticles: a Raman spectroscopic investigation *J. Appl. Phys.* 132 215107
- [38] Bhattacharjee S and Chattopadhyay K K 2023 Laser-induced Fano interference subsumed by electron-phonon coupling in orthorhombic KNbO3 nano-bricks: an ab initio vibrational and Raman spectroscopic investigation J. Raman Spectrosc. 54 871–86
- [39] Olego D, Cardona M and Vogl P 1982 Pressure dependence of the optical phonons and transverse effective charge in 3C-SiC Phys. Rev. B 25 3878–88
- [40] Feldman D W, Parker J H, Choyke W J and Patrick L 1968 Raman scattering in 6HSiC Phys. Rev. 170 698-704
- [41] Patrick L 1968 Infrared absorption in SiC polytypes Phys. Rev. 167 809
- [42] Salvador G and Sherman W 1991 Pressure dependence of the Raman phonon spectrum in 6h-silicon carbide J. Mol. Struct. 247 373-84
- [43] Sugie R, Uchida T, Kosaka K and Matsumura K 2016 Characterization of process-induced defects in SiC MOSFETs by cross-sectional cathodoluminescence *Jpn. J. Appl. Phys.* 55 04ER3
- [44] Olego D and Cardona M 1982 Pressure dependence of Raman phonons of Ge and 3 C-SiC Phys. Rev. B 25 1151
- [45] Balkanski M, Wallis R and Haro E 1983 Anharmonic effects in light scattering due to optical phonons in silicon Phys. Rev. B 28 1928
- [46] Debernardi A, Ulrich C, Syassen K and Cardona M 1999 Raman linewidths of optical phonons in 3 C—SiC under pressure: first-principles calculations and experimental results Phys. Rev. B 59 6774
- [47] Burton J, Sun L, Long F, Feng Z and Ferguson I 1999 First-and second-order Raman scattering from semi-insulating 4 H SiC Phys. Rev. B 59 7282
- [48] Mao H K, Xu J and Bell P M 1986 Calibration of the ruby pressure gauge to 800 kbar under quasi-hydrostatic conditions J. Geophys. Res. 91 4673–6
- [49] Schmidt C, Steele-MacInnis M, Watenphul A and Wilke M 2013 Calibration of zircon as a Raman spectroscopic pressure sensor to high temperatures and application to water-silicate melt systems *Am. Mineral.* 98 643–50
- [50] Schmidt C and Ziemann M A 2000 In-situ Raman spectroscopy of quartz: a pressure sensor for hydrothermal diamond-anvil cell experiments at elevated temperatures Am. Mineral. 85 1725–34
- [51] Datchi F and Canny B 2004 Raman spectrum of cubic boron nitride at high pressure and temperature Phys. Rev. B 69 144106
- [52] Datchi F, Dewaele A, Loubeyre P, Letoullec R, Le Godec Y and Canny B 2007 Optical pressure sensors for high-pressure-high-temperature studies in a diamond anvil cell High Pressure Res. 27 447–63
- [53] Schiferl D et al 1997 The diamond 13 C/12 C isotope Raman pressure sensor system for high-temperature/pressure diamond-anvil cells with reactive samples J. Appl. Phys. 82 3256–65
- [54] Fujimori H, Komatsu H, Ioku K, Goto S and Yoshimura M 2002 Anharmonic lattice mode of Ca2SiO4: ultraviolet laser Raman spectroscopy at high temperatures Phys. Rev. B 66 064306
- [55] Gillet P, Le Cléac'h A and Madon M 1990 High-temperature raman spectroscopy of SiO2 and GeO2 Polymorphs: anharmonicity and thermodynamic properties at high-temperatures *J. Geophys. Res.* 95 21635-55
- [56] Xu K 2021 Silicon electro-optic micro-modulator fabricated in standard CMOS technology as components for all silicon monolithic integrated optoelectronic systems J. Micromech. Microeng. 31 054001
- [57] Park C H, Cheong B-H, Lee K-H and Chang K J 1994 Structural and electronic properties of cubic, 2H, 4H, and 6H SiC Phys. Rev. B 49 4485–93
- [58] Bundy F P, Bassett W A, Weathers M S, Hemley R J, Mao H K and Goncharov A F 1996 The pressure–temperature phase and transformation diagram for carbon; updated through 1994 *Carbon* 34 141–53